Elasto-plastic behaviour of perforated steel plates subjected to compression and bending

Emanuele Maiorana, Carlo Pellegrino* and Claudio Modena

Department of Structural and Transportation Engineering, University of Padova, Via Marzolo 9, 35131 Padova, Italy

(Received April 13, 2010, Accepted February 14, 2011)

Abstract. The aim of this work is to provide some insights into the elasto-plastic behaviour of plate girder web square and rectangular panels with centred and eccentric holes under both compression and in-plane bending moment. The numerical study was validated comparing the numerical results obtained for one simple steel plate configuration with the corresponding experimental results, obtained at the University of Padova, observing the influence of the initial out-of-plane imperfections on the force vs. displacement relationship and ultimate strength. Once validated the numerical approach, the effect of bending moment on the stability of the plate is studied and some differences with respect to the uniform compression load case are shown. The influence of dimension and position of the hole, the plate aspect ratio and the steel grade on elasto-plastic behaviour is observed. Some indications regarding the critical slenderness (at which transition from elastic to plastic collapse occurs) are given for square and rectangular plates with symmetric and eccentric holes having small, medium and large diameter.

Keywords: steel girder; perforated plate; elasto-plastic analysis; in-plane loading.

1. Introduction

The problem of plate stability is of particular interest for steel structures particularly bridges. Holes are often unavoidable in webs of steel beams and in plates, due to inspection, maintenance and also aesthetic purposes. In these situations, presence of holes may cause redistribution of plane stresses in plates with a significant reduction of stability. Considerable research on perforated thin plates has been conducted by Roberts and Azizian (1984) about buckling and elasto-plastic collapse, Cheng and Fan (2001) about non-linear theory, and Shanmugam *et al.* (1999) about axially compressed perforated plates. Shanmugam *et al.* (2002) gave some insights on Finite Element modelling, Azhari *et al.* (2005) about local buckling and El-Sawy and Martini (2007) about stability of bi-axially loaded rectangular plates. Bedair (1997) studied the influence of in-plane restraint, Brown (1990) the concentrated loads, and Brown *et al.* (1987) the rectangular holes. Other contributions were given by Durban and Zuckerman (1999) about biaxial compression/tension, Narayanan and Chow (1984) about ultimate capacity of uniaxially compressed perforated plates, Narayanan and Darwish (1985) about strength of slender webs having eccentric holes and Pellegrino *et al.* (2009) about behaviour of perforated plates under shear loading.

The works of El-Sawy and Martini (2001) and El-Sawy *et al.* (2004) describe the results of an

* Corresponding author, Assistant Professor, E-mail: carlo.pellegrino@unipd.it

extensive research into linear and non-linear buckling analysis of perforated plates with uniformly distributed loads and the works of Maiorana *et al.* (2008a) and Maiorana *et al.* (2009a) describes linear and non-linear behaviour of plates under localised symmetrical loads.

While a number of studies have been developed about linear buckling behaviour of steel plates without perforations, even subjected to patch loading and bending moment (Maiorana *et al.* 2008b), few works are available on perforated plates and the particular case of elasto-plastic behaviour of perforated plates under both axial compression and in-plane bending moment is not deeply investigated. The linear buckling analysis was treated in Maiorana *et al.* (2009b). Komur and Sonmez (2008a, 2008b) developed elastic buckling analyses of rectangular plates with a circular cutout under linearly varying in-plane normal load. This work shows some new insights if compared with Maiorana *et al.* 2009b and Komur and Sonmez (2008a, 2008b) since elasto-plastic behaviour is studied.

In this work the Straus7 FEM code (G + D Computing 2005) was used for a parametric investigation in the elasto-plastic field on perforated plates subjected to in plane loading derived from the combination of both axial forces and bending moments. Stress ratios $\psi = -1$ (pure bending), –0.5, 0, 0.5, 1 (pure compression) were considered (see Fig. 1). The elastic behaviour until buckling load was investigated by a linear buckling analysis whereas the plastic phase was studied by a non-linear large deflection analysis.

The parameters taken into account are those mainly influencing the post-critical behaviour of perforated panels and are: (a) diameter d and position e_x of the hole; (b) panel slenderness λ and aspect ratio α; (c) yielding stress of the material f_y. A36 steel with f_y = 248 N/mm^2, A50 with f_y = 345 N/mm^2 and A60 with f_y = 414N/mm^2 were considered and an elastic-perfectly plastic law was assumed for the analysis.

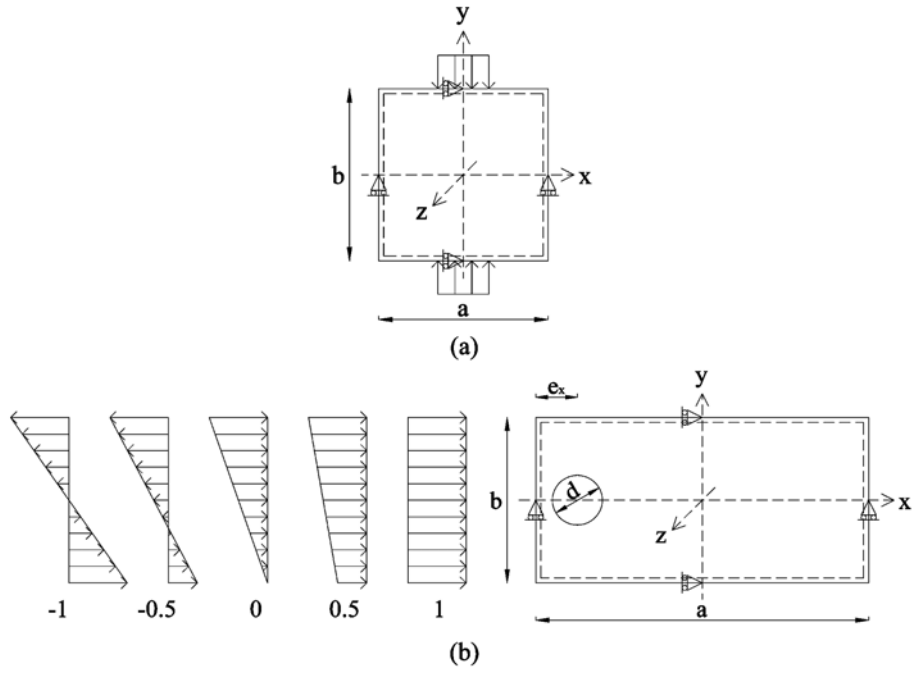

Fig 1. Loading scheme and boundary conditions for the validation (a) and the rest of the analyses (b).

Aspect ratios $a / b = 1$ (square plate), $a / b = 2$ and 3 (rectangular plates) and holes with small ($d/b = 0.1$), medium ($d/b = 0.3$) and large ($d/b = 0.5$) diameters were considered. The following hole positions were analysed: $e_x / b = 0.5$ for square plates, $e_x / b = 0.5$, 1 and 1.5 for rectangular plates. These positions are significant according to the critical deformed mode of the plate when subjected to uniform compression: they are the "nodal" point ($e_x / b = 1$) where the sinusoidal shape does not show any out-of-plane displacement and the "maximum" points ($e_x / b = 0.5$ and 1.5) where the sinusoidal shape shows the greatest value of the out-of-plane displacement (Maiorana *et al.* 2008a).

Critical slenderness (at which transition from elastic to elasto-plastic instability occurs) was calculated for square and rectangular plates with symmetric and eccentric holes having small, medium and large diameter when the stress ratio varies.

Linear buckling analyses were performed to obtain the elastic critical stress f_{cr} (corresponding to the critical value of σ_0) and compare this value with the yielding stress f_y on the basis of the ratio f_{cr} / f_y. If $f_{cr} / f_y > 1$, the failure of the plate is due to excessive steel yielding in the plastic field; if $f_{cr} / f_y < 1$, plate failure is due to instability and occurs in the elastic field (El-Sawy and Martini 2001). For thin plates (i.e., with high values of slenderness) instability occurs for elastic buckling stress f_{cr} less than yielding stress f_y, especially if the plate has small holes. On the contrary, instability could occur after material yielding in stocky plates (i.e., with low slenderness values) or perforated plates with large holes.

2. Validation of the procedure

A sensitivity analysis to define the shape and dimensions of the elements was developed and extensively described by the authors in Pellegrino *et al.* (2009). Discretizations with the following elements were considered: (a) square elements for the entire model except the zone around the hole, where trapezoidal elements with four nodes were used; (b) square elements for the entire model except the zone around the hole, where triangular elements with three nodes were used; (c) triangular elements for the entire model. Deformed shape and buckling coefficient are not significantly influenced by mesh element shape or size, so that plate elements with four nodes and six degrees of freedom for each node were used for the following analyses. The typical size of the element was about $b / 20$, and the elements along the perimeter and near the hole had dimensions of $b / 50$ or $\pi d / 40$ (see Fig. 2). Further details on the sensitivity analysis can be found in Pellegrino *et al.* (2009).

In order to validate the numerical approach and the discretization, a comparison between numerical

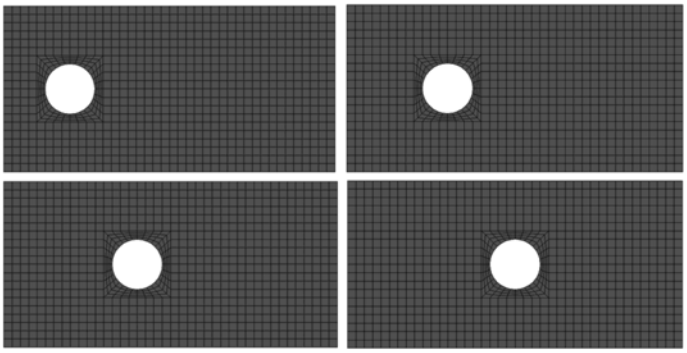

Fig 2. Sample mesh for rectangular plates with circular hole in different positions

and experimental results, in terms force vs. out-of-plane displacement diagram, obtained on panels tested at the Materials Testing Laboratory of the Department of Structural and Transportation Engineering, University of Padova, was developed.

The boundary conditions for the FE model used in the benchmarking are the same of the model used in the rest of the theoretical study. The only difference is the load configuration (localised load for the benchmarking and in-plane axial load plus bending moment for the rest of the study). In Fig. 1(a) boundary conditions and load configuration for the benchmarking and in Fig. 1(b) boundary conditions and load configuration for the rest of the analyses are shown. The four edges were simply supported in the out-of-plane direction, in-plane rigid movements were constrained by means of restraints located as shown in Fig. 1(a) and (b). The load was applied directly to the nodes as a system of conservative forces that do not change direction after the deformation.

Considering the non-linear buckling analyses developed in Maiorana *et al.* (2009c), it seems appropriate to assume the deformed shape, corresponding to the first buckling mode, as initial configuration of the panels with and without perforations to study their elasto-plastic behaviour since results in terms of ultimate load for actual panels with measured imperfections and numerically deformed ones were similar for each configuration of the load, dimension and position of the hole. In the non-linear analyses the magnitude of the initial deformation, derived from the linear buckling analysis, is less than $b/100$ since Maiorana *et al.* (2009c) showed that the influence of the initial deformation on the ultimate load is not significant when its magnitude is less than $b/100$.

The panel taken into consideration for the benchmarking is a square panel with dimensions $a = b = 500$ mm and thickness $t = 5$ mm (slenderness $\lambda = 100$). Carbon steel grade S355J0 with Young's modulus $E = 206000$ N/mm^2 and Poisson's ratio $v = 0.3$ was used.

The test regards a panel similar to those studied in the paper. The only difference is the load condition: in-plane symmetrical localized load is applied in the experimental investigation and in-plane compression and bending was applied in the numerical study. This is due to the practical difficulty to apply both in-plane compression and bending to the specimens during the experimental tests. Nevertheless the experimental results can be used to validate the numerical approach even if the load configuration was different.

The length of the localised load was kept constant (ratio between length of the load and dimension of the panel $s_s / a = 0.2$). The tests on the panels were carried out monotonically, under a 10000 kN loading capacity machine, with loads increased between 0.5 and 2.5 kN/s. Pressure transducer mounted on the loading machine was used to measure the applied loads. The panels were instrumented with a number of linear variable differential transducers (LVDT) placed orthogonally to the web to measure out-of-plane web displacements.

Fig. 3 shows a synthesis of the comparison between numerical and experimental results: Fig. 3(a) shows the numerical and experimental deformed shapes at 25% and at 100% of the ultimate load, Fig. 3b the static scheme with the location of the measurement points, Fig. 3(b) the experimental force vs. displacement diagram in one significant point compared with the numerical one obtained with an initial deformed configuration corresponding to the first buckling mode with different maximum initial out-of-plane displacements (1.25 mm, 2.5 mm and 5 mm).

It can be observed that the numerical results are in good agreement with the experimental ones both in terms of out-of-plane deformed shape (Fig. 3(a)) and load vs. out-of-plane displacement diagram with a small influence of the amplitude of the considered initial imperfection (Fig. 3(c)).

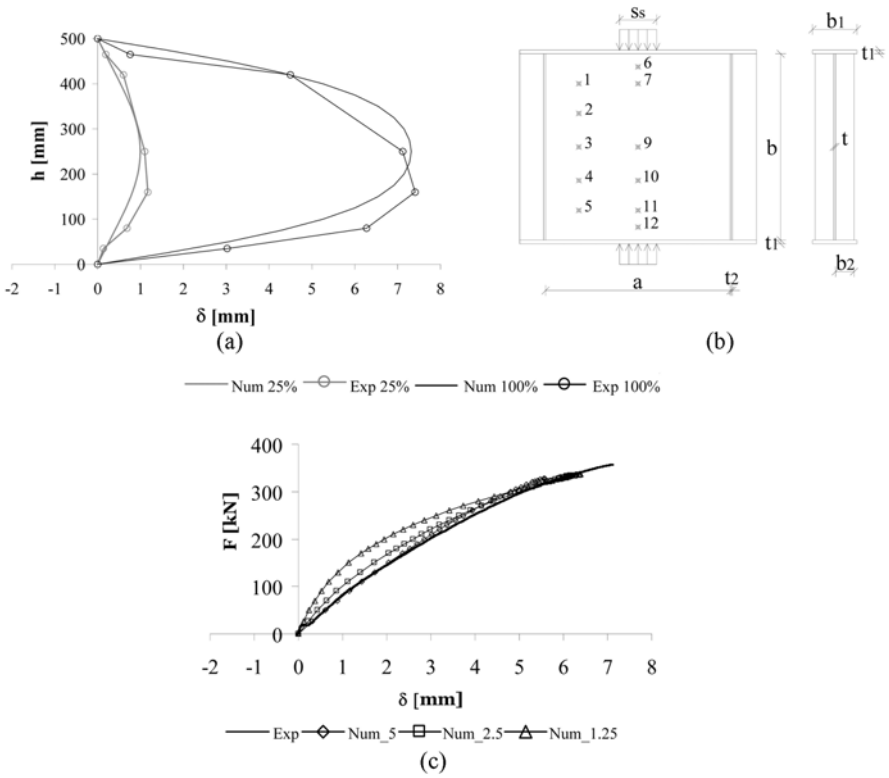

Fig 3. Validation of the numerical model. (a) numerical and experimental deformed shape at 25% and 100% of the ultimate load; (b) static scheme with measurement points; (c) numerical (with various values of the initial imperfections) and experimental force vs. displacement diagram for point n. 9

3. Square plates

In the following f_{cr} / f_y vs. λ diagrams are shown for square plates ($a / b = 1$) with small, medium and large holes ($d / b = 0.1$, 0.3 and 0.5), located in the centre of the plate ($e_x / b = 0.5$) subjected to pure in-plane bending ($\psi = -1$), combination of axial compression and bending ($\psi = -0.5$, 0 and 0.5) and pure compression ($\psi = 1$). A36, A50 and A60 steel plates were considered.

Fig. 4 shows, as an example, f_{cr} / f_y vs. λ diagrams for A36 ($f_y = 248$ N/mm^2) steel square plates with circular holes having $d / b = 0.1$ and 0.5 located in the centre of the panel ($e_x / b = 0.5$). The grey curves are obtained with linear buckling analysis, the black curves with non-linear analysis.

The diagrams in Fig. 4 have similar trends with progressive reduction of f_{cr} / f_y when λ increases. For $\lambda < \lambda_{cr}$, where λ_{cr} is the critical slenderness at which transition between elastic and elasto-plastic fields is observed, failure in plastic field occurs. Critical stresses are minor for large holes ($d / b = 0.5$) than for small holes ($d / b = 0.1$): the increase of d / b causes the reduction of the stability. The plastic field, in which the collapse occurs for steel yielding, increases with the reduction of since the collapse is due to excessive plasticization for pure bending ($\psi = -1$). In the case of the $\psi = -1$, the elasto-plastic curves are the same for different hole dimensions, hence, for pure bending, the diameter of y the hole does not influence the critical stress of the plate. Such behaviour is due to the position of the hole in relation to the stress ratio, since the effect of the applied load is small at the centre of the plate, where

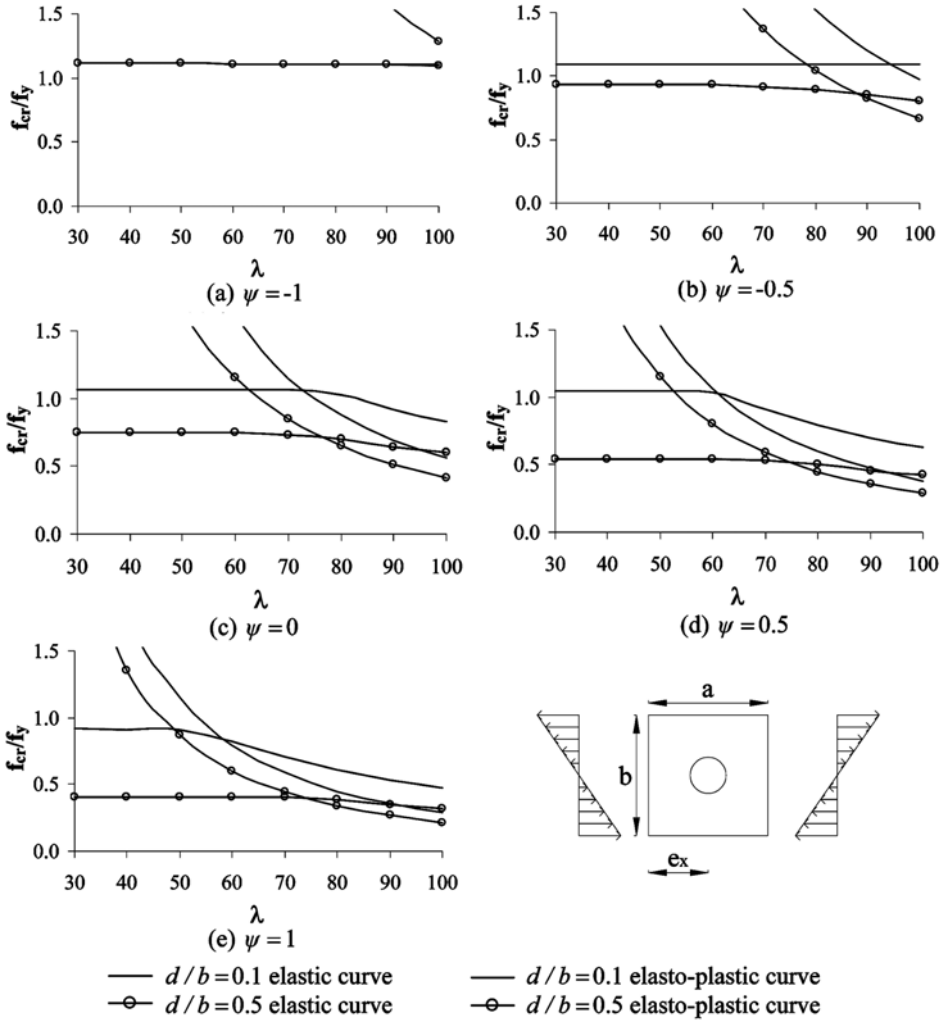

Fig 4. f_{cr} / f_y vs. λ diagrams for square plates and hole in $e_x / b = 0.5$; A36 steel

the hole is located, while it becomes maximum near the compression and tension edges, where the plate has a solid continuous strip capable of carrying the load. The difference between the elasto-plastic curves corresponding to small and large hole diameters increases with y and for pure compression (y =1) the maximum stress is in the perforated zone.

For $\psi = -0.5$ holes with $d / b = 0.1$ do not substantially influence the collapse of the plate for the considered slenderness range; holes with major dimension ($d / b = 0.5$), instead, influence the failure mode of the plate. The opposite situation occurs for uniform compression ($\psi = 1$) for which every hole size strongly influences the failure mode even for smaller slenderness. Both curves, due to linear and non-linear buckling analyses, become closer when ψ and λ increase.

For A50 ($f_y = 345$ N/mm^2) steel square plates with circular holes having $d / b = 0.1$ and 0.5 located in the centre of the panel, lower values of the ratio f_{cr} / f_y (with respect to A36 steel) are generally obtained for each hole size with non-linear analysis; the curves obtained with the linear buckling analysis do not depend on steel grade.

Furthermore, for A60 (f_y = 414 N/mm^2) steel square plates with circular holes located in the centre of the panel, lower values of the ratio f_{cr} / f_y (with respect to A36 and A50 steel) are generally obtained with elasto-plastic analyses.

Less sudden plastic collapse occurs and post-critical mechanisms develop in steel plates with reduced yielding strength.

Fig. 5 shows the limit between the elastic and plastic field in a d / b vs. λ diagram for square plates and A36, A50 and A60 steel. The hole is located in $e_x / b = 0.5$. The diagram for $\psi = -1$ shows only the curve for A60 steel because the curves for A36 and A50 steel are out of scale.

Critical slenderness reduces when steel grade and ψ increases.

For holes with $d / b = 0.1$ the critical slenderness λ_{cr} does not vary with respect to the corresponding unperforated plate since the distribution of stresses does not significantly vary. For holes with $d / b = 0.3$, when $\psi = 1$ and 0, λ_{cr} is the same of the plates with $d / b = 0.1$ and without holes. For with $d / b = 0.3$, when $\psi = -0.5$, λ_{cr} is instead significantly minor than the corresponding case of holes with $d / b = 0.1$ due to the variation of the distribution of the plate stresses. For holes $d / b = 0.5$, an increase of

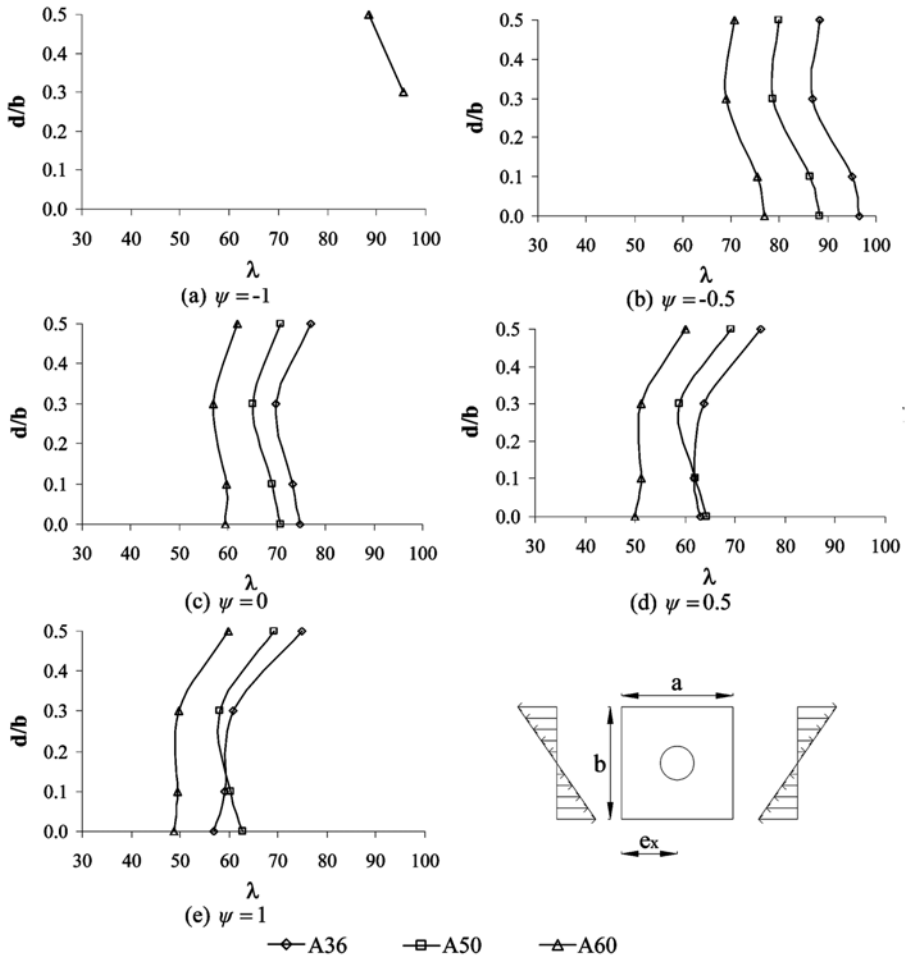

Fig 5. Elastic and plastic fields for square plates and hole in $e_x / b = 0.5$; A36, A50 and A60 steel

λ_{cr} and consequently widening of the plastic field occurs. In this case, the reduced amplitude of the zone between hole edge and loaded edge make the plate more prone to yield rather than buckle even for relatively high slenderness.

Some slenderness limits, below which plastic collapse occurs, are found for various found for various load conditions and hole dimensions. For small diameters: $\lambda = 88$ for $\psi = -1$, $\lambda = 68$ for $\psi = -0.5$, $\lambda = 56$ for $\psi = 0$, $\lambda = 50$ for $\psi = 0.5$ and $\lambda = 48$ for $\psi = 1$.

4. Rectangular plates

4.1 Plates with $a / b = 2$ and eccentric hole in $e_x / b = 0.5$

Fig. 6 shows f_{cr} / f_y vs. λ diagrams for A50 steel rectangular plates with $a / b = 2$ and circular holes, having $d / b = 0.1$ and 0.5, located in the centre of the first sub-panel ($e_x / b = 0.5$), subjected to pure bending ($\psi = -1$), combined compression and bending ($\psi = -0.5$, 0 and 0.5) and uniform axial compression ($\psi = 1$). The grey curves are obtained with linear buckling analysis, the black curves with non-linear analysis.

The behaviour of the rectangular plate with eccentric (located in the centre of the sub-panel) hole is similar to that of the square plate, with the only difference consisting in major resistance in the plastic field given by the adjacent whole sub-panel.

Fig. 7 shows the limit between the elastic and plastic field in a d / b vs. λ diagram for rectangular plates with $a / b = 2$, eccentric hole ($e_x / b = 0.5$), and A50 steel. Load conditions are combined compression and bending ($\psi = -0.5$, 0 and 0.5) and uniform axial compression ($\psi = 1$). The diagram for $\psi = -1$ (pure bending) is not included because it is out of scale.

Comparing with square plates, an increment of λ_{cr} , and the consequent increase of the plastic field amplitude, is observed for holes with $d / b = 0.3$ and 0.5. This is due to the major resistance in the plastic field given by the adjacent whole sub-panel.

Some slenderness limits for A50 steel, below which plastic collapse occurs, are found for various load conditions and hole dimensions. For small diameters: $\lambda = 83$ for $\psi = -0.5$, $\lambda = 69$ for $\psi = 0$, $\lambda = 62$ for $\psi = 0.5$ and $\lambda = 61$ for $\psi = 1$.

4.2 Plates with $a / b = 2$ and centred hole with $e_x / b = 1$

Fig. 8 shows f_{cr} / f_y vs. λ diagrams for A50 steel rectangular plates with $a / b = 2$ and circular holes, having $d / b = 0.1$ and 0.5, located in the centre of the plate between the first and the second sub-panels ($e_x / b = 1$), with stress ratios $\psi = -1$, -0.5, 0, 0.5, and 1.

Comparing with the corresponding diagrams for square plates and rectangular plates with $a / b = 2$ and eccentric hole in $e_x / b = 0.5$ (Fig. 6), the curves in Fig. 8 are less steep with higher values of the ratio f_{cr} / f_y, particularly for plates with hole $d / b = 0.5$. The greater distance of the hole from the loaded edge, with respect to the case of eccentric hole, allows more pronounced stress redistribution and a reduction of stress concentrations near loaded edges; this circumstance means that the plate is, in this last case, less prone to buckling.

The curves obtained with linear buckling analysis for holes with $d / b = 0.1$ and 0.5 are closer than the above cases confirming that the dimension of the hole has less influence for the stability of the plate if the hole is in the "nodal" point of the critical deformed shape (the "nodal point" is assumed as the

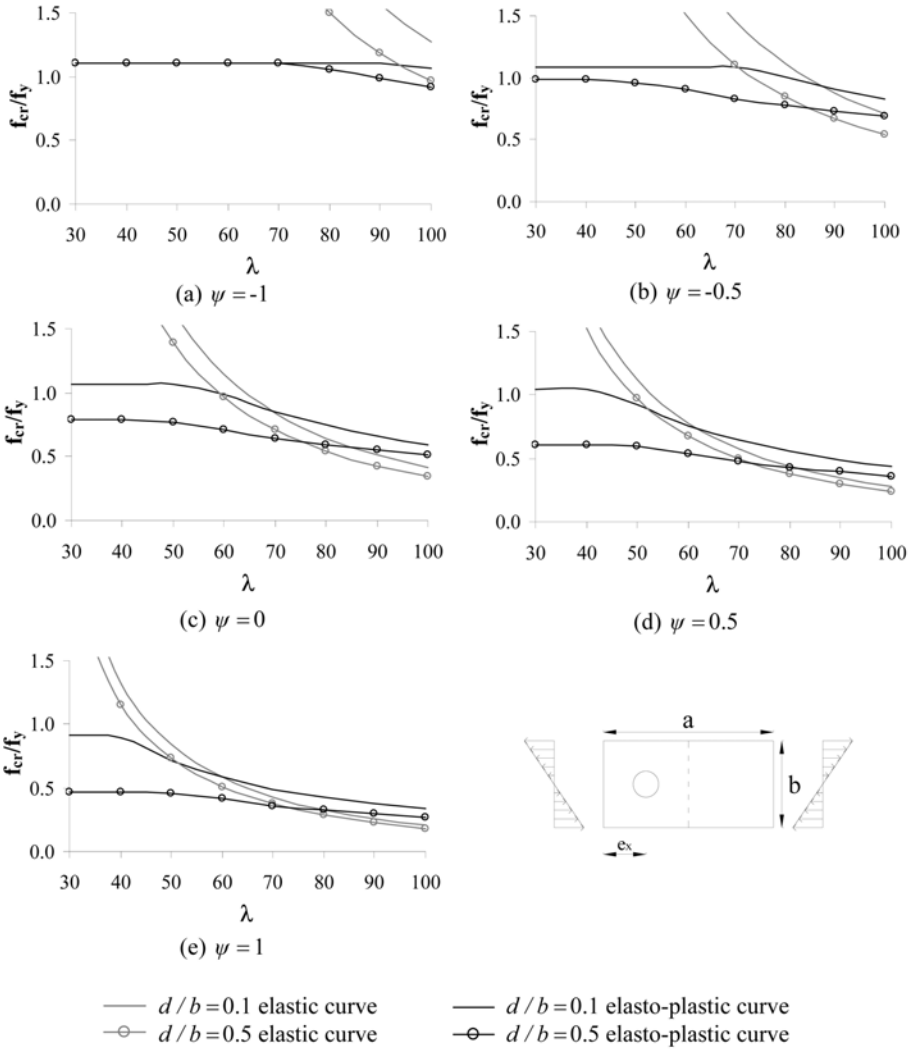

Fig 6. f_{cr} / f_y vs. λ diagrams for rectangular plates with $a / b = 2$ and hole in $e_x / b = 0.5$; A50 steel

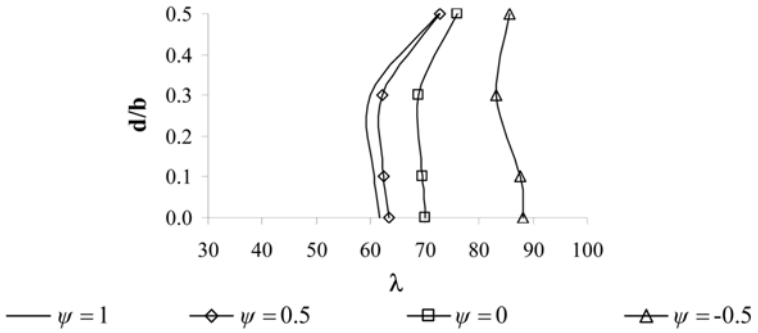

Fig 7. Elastic and plastic fields for rectangular plates with $a / b = 2$ and hole in $e_x / b = 0.5$; A50 steel

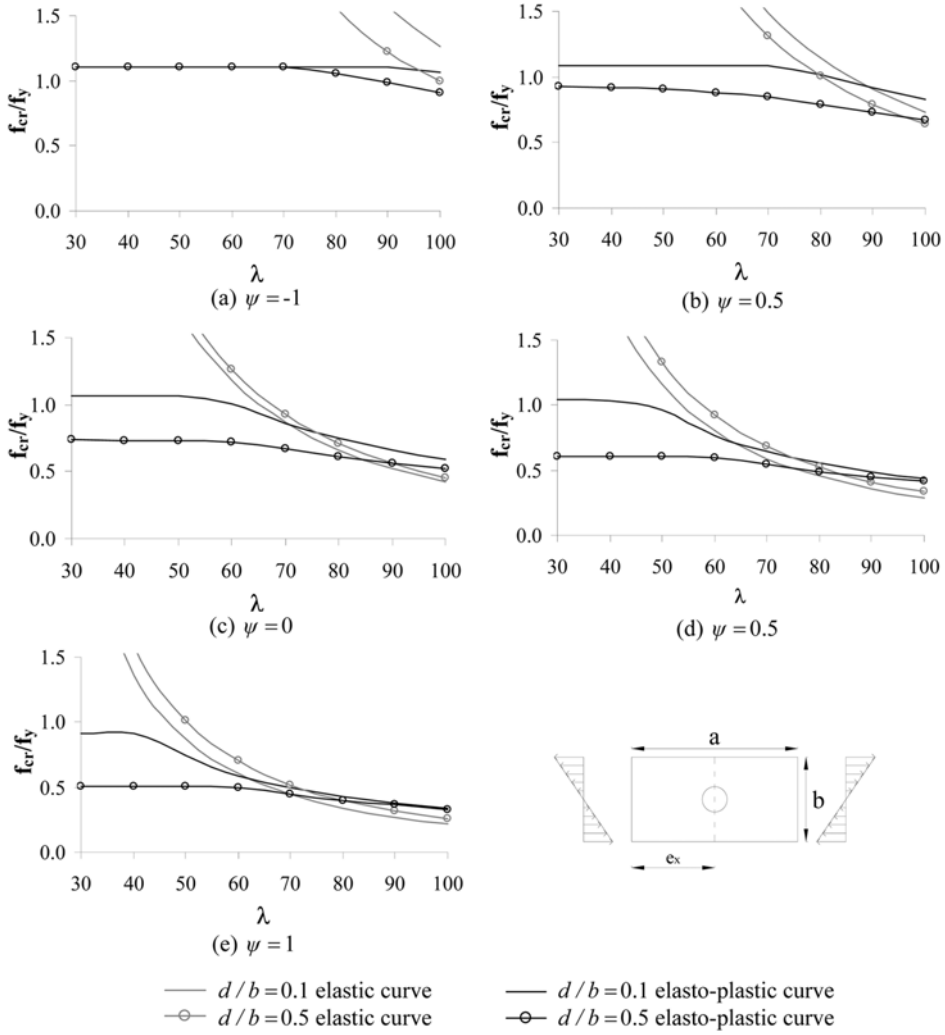

Fig 8. f_{cr} / f_y vs. λ diagrams for rectangular plates with $a / b = 2$ and hole in $e_x / b = 1$; A50 steel

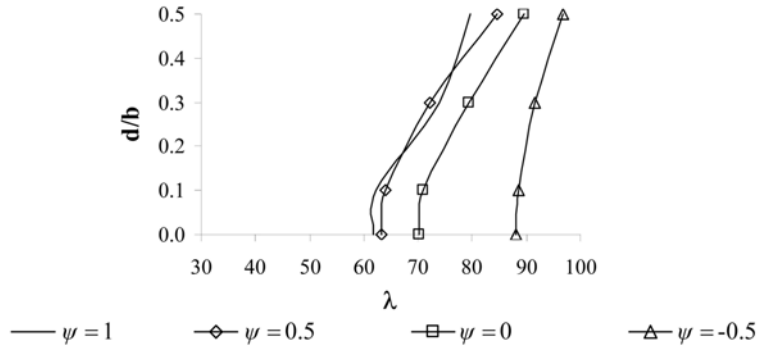

Fig 9. Elastic and plastic fields for rectangular plates with $a / b = 2$ and hole in $e_x / b = 1$; A50 steel

position where the sinusoidal shape does not show any out-of-plane displacement).

Fig. 9 shows the limit between the elastic and plastic field in a d / b vs. λ diagram for rectangular plates with $a / b = 2$, centred hole ($e_x / b = 1$), and A50 steel. Stress ratios $\psi = -0.5$, 0, 0.5 and 1 are again considered. The diagram for $\psi = -1$ is not included because it is out of scale.

Smallest critical slenderness always corresponds to unperforated plates; this circumstance does not always occur in the previous cases. In this case the increase of the hole diameter causes the increase of the critical slenderness.

Comparing elastic and plastic fields for rectangular plates with $a / b = 2$ and centred hole in $e_x / b = 1$ (Fig. 9) with corresponding plates having eccentric hole in $e_x / b = 0.5$ (Fig. 7), a reduction of the elastic field is observed for centred hole ($e_x / b = 1$), particularly for holes with $d / b = 0.3$ and 0.5; this confirms the major stability of the plate with centred hole.

Some slenderness limits for A50 steel, below which plastic collapse occurs, are found for rectangular plates with $a / b = 2$ and centred small hole in $e_x / b = 1$: $\lambda = 88$ for $\psi = -0.5$, $\lambda = 70$ for $\psi = 0$, $\lambda = 63$ for $\psi = 0.5$ and $\lambda = 61$ for $\psi = 1$.

4.3 Plates with a / b = 3 and hole with e_x / b = 0.5, 1 and 1.5

Fig. 10 shows f_{cr} / f_y vs. λ diagrams for A50 steel rectangular plates with $a / b = 3$ and circular holes, having $d / b = 0.1$ and 0.5, located in the centre of the first sub-panel ($e_x / b = 0.5$), with stress ratios $\psi = -1$, -0.5, 0, 0.5, and 1.

The comments are similar to those following Fig. 6 (plate with $a / b = 2$ and hole in $e_x / b = 0.5$).

Fig. 11 shows the limit between the elastic and plastic field in a d / b vs. λ diagram for rectangular plates with $a / b = 3$, hole in $e_x / b = 0.5$, and A50 steel. Stress ratios $\psi = -0.5$, 0, 0.5 and 1 are again considered.

Some slenderness limits for A50 steel are found for rectangular plates with $a / b = 3$ and hole in $e_x / b = 0.5$: $\lambda = 84$ for $\psi = -0.5$, $\lambda = 69$ for $\psi = 0$, $\lambda = 63$ for $\psi = 0.5$ and $\lambda = 60$ for $\psi = 1$.

Fig. 12 shows f_{cr} / f_y vs. λ diagrams for rectangular plates with circular holes between the first and the second sub-panel ($e_x / b = 1$).

The comments are similar to those following Fig. 8 (plate with $a / b = 2$ and hole in $e_x / b = 1$). Critical stresses obtained for plates with $a / b = 3$ are higher than those for plates with $a / b = 2$ due to major reserve of strength of the longer plate in plastic phase.

Fig. 13 shows elastic and plastic fields in a d / b vs. λ diagram for $e_x / b = 1$. Critical slenderness for plates with $a / b = 3$ are lower than those of the corresponding plates with $a / b = 2$ and hole in $e_x / b = 1$, for $d / b = 0.3$ and 0.5 (see Fig. 9). Hence an increase of the elastic field amplitude occurs when the aspect ratio a / b increases.

Slenderness limits for rectangular plates with $a / b = 3$ and hole in $e_x / b = 1$ (A50 steel) are the same of the plates with $a / b = 2$ and hole in $e_x / b = 1$ (Fig. 9).

Fig. 14 shows f_{cr} / f_y vs. λ diagrams for rectangular plates with $a / b = 3$ and circular holes, having $d / b = 0.1$ and 0.5, with the centre in the second sub-panel ($e_x / b = 1.5$).

Critical stresses obtained for plates with $a / b = 3$ and hole in $e_x / b = 1.5$ are near to those for plates with $a / b = 3$ and $e_x / b = 0.5$ (see Fig. 10). Both the positions of the centre of the hole correspond, for the considered load conditions, to "maximum" points (assumed as the position where the sinusoidal shape shows the maximum out-of-plane displacement) of the critical deformed shape of the unperforated plate. This is the worst position of the hole as regards stability behaviour. The increase of the critical stresses from hole in $e_x / b = 0.5$ to hole in $e_x / b = 1.5$ is due to the fact that the hole is far

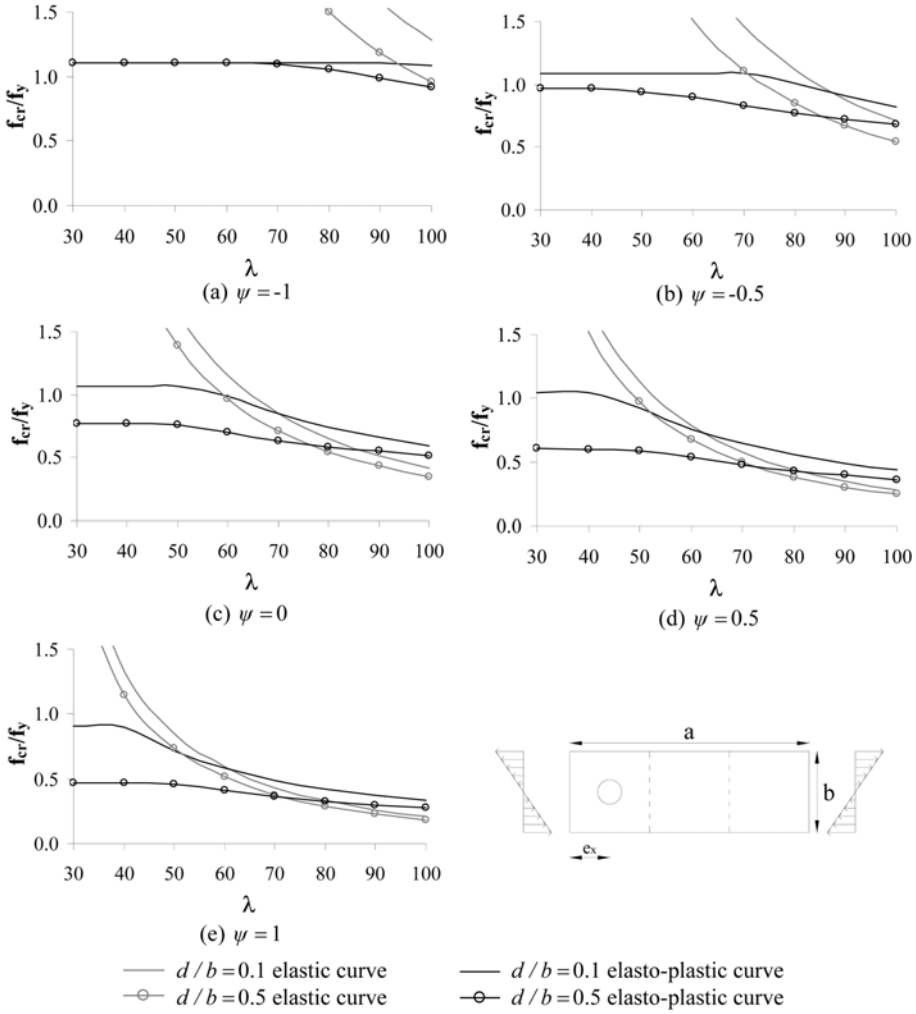

Fig 10. f_{cr} / f_y vs. λ diagrams for rectangular plates with $a / b = 3$ and hole in $e_x / b = 0.5$; A50 steel

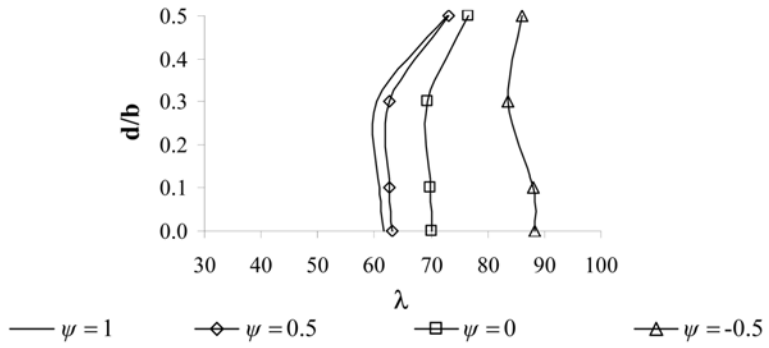

Fig 11. Elastic and plastic fields for rectangular plates with $a / b = 3$ and hole in $e_x / b = 0.5$; A50 steel

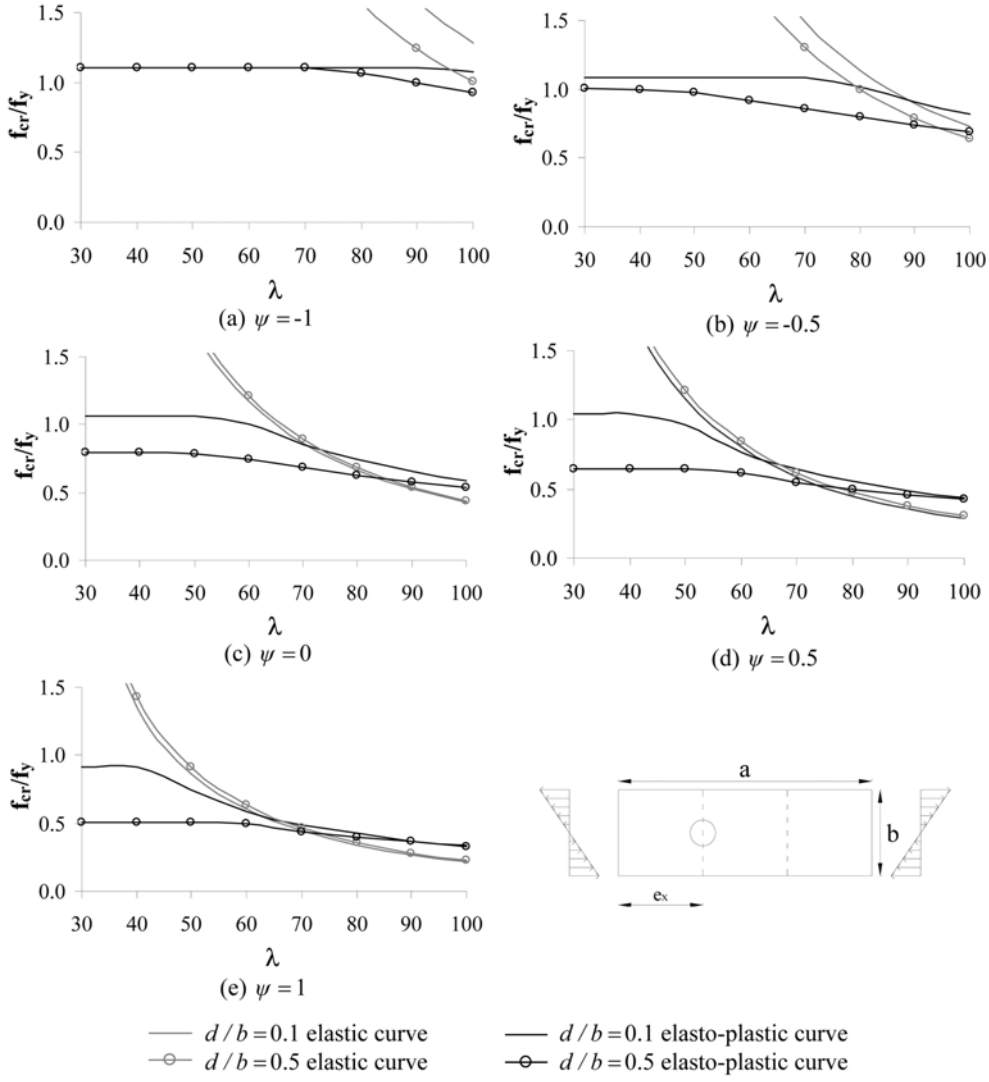

Fig 12. f_{cr} / f_y vs. λ diagrams for rectangular plates with $a / b = 3$ and hole in $e_x / b = 1$; A50 steel

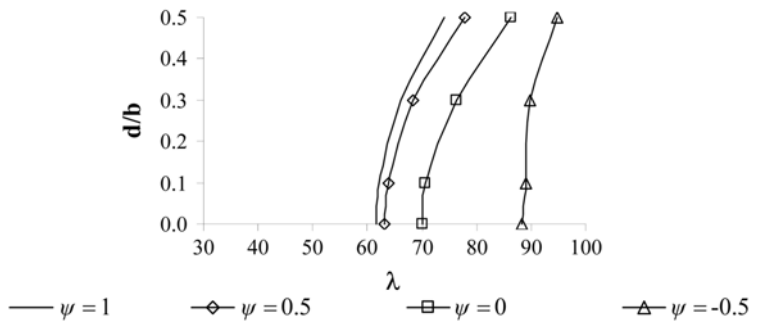

Fig 13. Elastic and plastic fields for rectangular plates with $a / b = 3$ and hole in $e_x / b = 1$; A50 steel

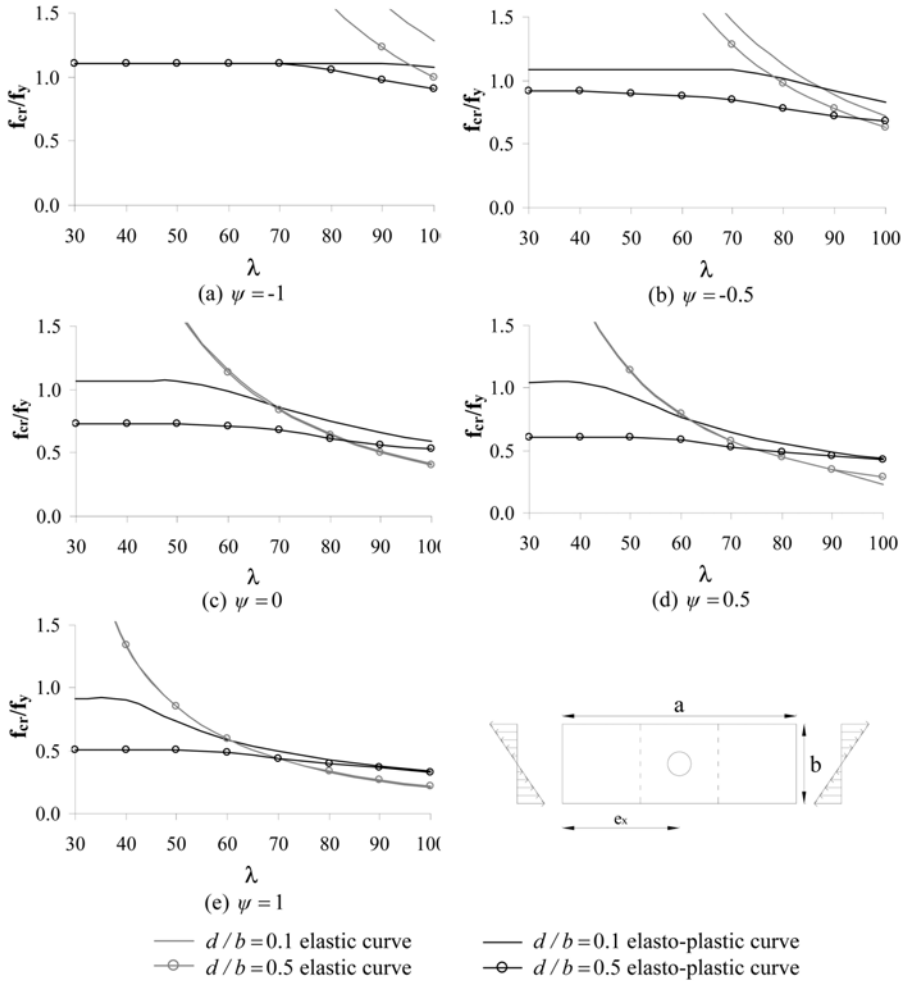

Fig 14. f_{cr} / f_y vs. λ diagrams for rectangular plates with $a / b = 3$ and hole in e_x / b 1.5; A50 steel

from the loaded edge when $e_x / b = 1.5$.

Critical stresses obtained for plates with $a / b = 3$ and hole in $e_x / b = 1.5$ are near to those for plates with $a / b = 3$ and $e_x / b = 1$ (see Fig.12) Although the geometric configuration of hole in $e_x / b = 1$ corresponds to a "nodal" point (assumed as the position where the sinusoidal shape does not show any out-of-plane displacement). Holes having the centre in "nodal" points have a reduced influence on the stability of the plate.

Fig. 15 shows elastic and plastic fields in a d / b vs. λ diagram for $e_x / b = 1.5$. Critical slenderness for plates with $a / b = 3$ and centred hole in $e_x / b = 1.5$ are lower than those of the corresponding plates with $a / b = 3$ and hole in $e_x / b = 1$ (Fig. 13) for holes with $d / b = 0.3$ and 0.5. Hence an increase of the elastic field amplitude occurs, for rectangular plates with $a / b = 3$, when the hole moves towards the centre of the plate. Critical slenderness for plates with $a / b = 3$ and centred hole in $e_x / b = 1.5$ are higher than those of the corresponding plates with $a / b = 3$ and hole in $e_x / b = 0.5$ (Fig. 11) for holes with $d / b = 0.3$ and 0.5. The critical slenderness, instead, does not vary for plates with hole size $d / b = 0.1$ with respect to the unperforated plate.

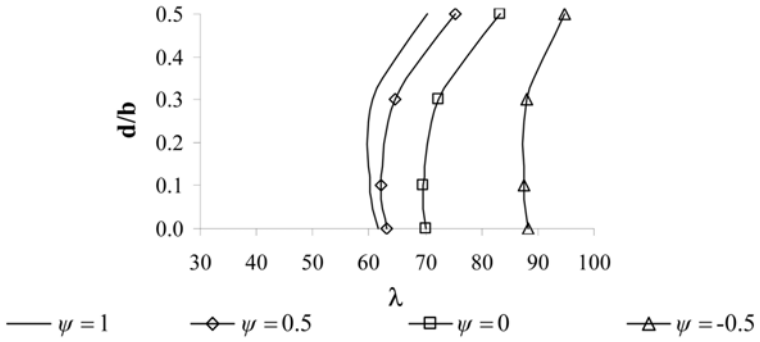

Fig 15. Elastic and plastic fields for rectangular plates with $a / b = 3$ and hole in 1.5; A50 steel

Slenderness limits for rectangular plates with $a / b = 3$ and small hole in $e_x / b = 1.5$ (A50 steel) are as follows: $\lambda = 88$ for $\psi = -0.5$, $\lambda = 70$ for $\psi = 0$, $\lambda = 62$ for $\psi = 0.5$ and $\lambda = 60$ for $\psi = 1$.

5. Conclusions

In this work the elasto-plastic behaviour of plate girder web square and rectangular panels with centred and eccentric holes under both compression and bending moment was studied.

In order to validate the numerical approach, a comparison between numerical and experimental results, in terms of force vs. out-of-plane displacement diagram and deformed shape, obtained on panels tested at the University of Padova, was developed and a good agreement was obtained.

The influence of the following parameters on stability and elasto-plastic collapse was numerically investigated:

- shape of the plate (square – $a / b = 1$ – and rectangular – $a / b = 2, 3$);
- steel grade (A36, A50, and A60 with $f_y = 248$, 345 and 414 N/mm^2 respectively);
- dimension ($d / b = 0.1$, 0.3, and 0.5) and position of the circular hole ($e_x / b =$ ratio);
- load configuration corresponding to uniform compression ($\psi = 1$), combination of axial force and bending moment ($\psi = 0.5$, 0 and –0.5) and pure bending ($\psi = -1$).

The following conclusions can be drawn.

- Elastic curves of plates with different hole dimensions become closer when stress ratio ψ increases while distance between elasto-plastic curves of plates with different hole dimensions increases when stress ratio ψ increases.
- Plastic field reduces (critical slenderness decreases) when ψ increases.
- The increase of the hole size causes the reduction of the plastic strength.
- Rectangular perforated plates show more pronounced plastic behaviour than square plates (depending on hole position).
- Rectangular plates with the centre of the hole in the "maximum" point of the critical deformed shape of the corresponding unperforated plate, far from the loaded edge, show major stability and higher plastic strength than square plates. Any appreciable differences have been observed between square and rectangular plates with hole in $e_x / b = 0.5$ (near the loaded edge).
- Plates with the centre of the hole in the "nodal" point of the critical deformed shape show major stability and higher plastic strength than plates having the centre of the hole is in the "maximum" point of the critical deformed shape.

Acknowledgements

The writers wish to thank OMBA Impianti & Engineering SpA of Torri di Quartesolo(Vicenza, Italy) for supplying the panel for the validation of the numerical approach and Mr I. Simion and Mr E. Mazzocato for contributing to some numerical analyses developed during the thesis.

References

Azhari, M., Shahidi, A.R. and Saadatpour, M.M. (2005), "Local and post local buckling of stepped and perforated thin plates", *Appl. Math. Model.*, **29(7)**, 633-52.

Bedair, O.K. (1997), "Influence of in-plane restraint on the buckling behaviour of plates under uniform compression, shear and in-plane bending", *Comp. Meth. Appl. Mech. Eng.*, **148**, 1-10.

Brown, C.J. (1990), "Elastic buckling of perforated plates subjected to concentrated loads", *Comp. Struct.*, **36(6)**, 1103-9.

Brown, C.J., Yettram, A.L. and Burnett, M. (1987), "Stability of plates with rectangular holes", *J. Struct. Eng.*, ASCE, **113(5)**, 1111-6.

Cheng, C.J. and Fan, X.J. (2001), "Nonlinear mathematical theory of perforated viscoelastic thin plates with its applications", *Inter. J. Solids. Struct.*, **38(36)**, 6627-41.

Durban, D. and Zuckerman, Z. (1999), "Elasto-plastic buckling of rectangular plates in biaxial compression/ tension", *Int. J. Mech. Sci.*, **41**, 751-65.

El-Sawy, K.M. and Martini, M.I. (2001), "Effect of aspect ratio on the elastic buckling of uniaxially loaded plated with eccentric holes", *Thin. Walled. Struct.*, **39(12)**, 983-98.

El-Sawy, K.M., Nazmy, A.S. and Martini, M.I. (2004), "Elasto plastic buckling of perforated plates under uniaxial compression", *Thin. Walled. Struct.*, **42(8)**, 1083-101.

El-Sawy, K.M. and Martini, M.I. (2007), "Elastic stability of bi-axially loaded rectangular plates with a single circular hole", *Thin. Walled. Struct.*, **45(1)**, 122-33.

G+D Computing (2005), *Straus7 user's manual*, Sydney.

Komur, M.A. and Sonmez, M. (2008a), "Elastic buckling of rectangular plates under linearly varying in-plane normal load with a circular cutout", *Mech. Res. Communications.*, **35**, 361-71.

Komur, M.A. and Sonmez, M. (2008b), "Elastic buckling of perforated plates subjected to linearly varying in-plane loading". *Struct. Eng. Mech.*, **28(3)**, 353-356

Maiorana, E., Pellegrino, C. and Modena, C. (2008a), "Linear buckling analysis of perforated plates subjected to localised symmetrical load", *Engi. Struct.*, **30(11)**, 3151-8.

Maiorana, E., Pellegrino, C. and Modena, C. (2008b), "Linear buckling analysis of unstiffened plates subjected to both patch load and bending moment", *Eng. Struct.*, **30(12)**, 3731-8.

Maiorana, E., Pellegrino, C. and Modena, C. (2009a), "Non-linear analysis of perforated steel plates subjected to localised symmetrical load", *J. Const. Steel. Res.*, **65(4)**, 959-64.

Maiorana, E., Pellegrino, C. and Modena, C. (2009b), "Elastic stability of plates with circular and rectangular holes subjected to axial compression and bending moment", *Thin.Walled. Struct.*, **47(3)**, 241-55.

Maiorana, E., Pellegrino, C. and Modena, C. (2009c), "Imperfections in steel girder webs with and without perforations under patch loading", *J. Constr. Steel. Res.*, **65(5)**, 1121-9.

Narayanan, R. and Chow, F.Y. (1984), "Ultimate capacity of uniaxially compressed perforated plates", *Thin. Walled. Struct.*, **2(3)**, 241-64.

Narayanan, R. and Darwish, I.Y.S. (1985), "Strength of slender webs having non central holes", *Struct. Eng.*, **63B(3)**, 57-61.

Pellegrino, C., Maiorana, E. and Modena, C. (2009), "Linear and non-linear behaviour of perforated steel plates with circular and rectangular holes under shear loading", *Thin.Walled. Struct.*, **47(6-7)**, 607-616.

Roberts, T.M. and Azizian, Z.G. (1984), "Strength of perforated plates subjected to in-plane loading", *Thin. Walled. Struct.*, **2(2)**, 153-64.

Shanmugam, N.E., Thevendran, V. and Tan, Y.H. (1999), "Design formula for axially compressed perforated plates", *Thin. Walled. Struct.*, **34(1)**, 1-20.
Shanmugam, N.E., Lian, V.T. and Thevendran, V. (2002), "Finite element modelling of plate girders with web openings", *Thin. Walled. Struct.*, **40(5)**, 443-64.

CC

Appendix 1: Notation.

Symbol	Description
a	panel length
b	panel width
d	hole diameter
E	elastic Young's modulus of plate's material
F_u	ultimate load
f_{cr}	elastic critical stress
f_y	yielding stress
t	thickness of the panel
x	hole position along horizontal axis
α	aspect ratio of rectangular plate (a/b)
λ	plate slenderness (a/t)
λ_{cr}	critical slenderness at which buckling type changes from elastic to elasto-plastic
σ_0	reference stress value applied at panel ends
ψ	stress ratio of the linearly varying end stress
ν	Poisson's ratio of plate's material